Title	Effect of Salt on Dynamic Mechanical Behaviors of Polyampholyte Hydrogels
Author(s)	Li, Xueyu; Luo, Feng; Sun, Tao Lin; Cui, Kunpeng; Watanabe, Reina; Nakajima, Tasuku; Gong, Jian Ping
Citation	Macromolecules, 56(2), 535-544 https://doi.org/10.1021/acs.macromol.2c02003
Issue Date	2022
Doc URL	http://hdl.handle.net/2115/91075
Rights	This document is the Accepted Manuscript version of a Published Work that appeared in final form in Macromolecules, copyright © American Chemical Society after peer review and technical editing by the publisher. To access the final edited and published work see https://pubs.acs.org/articlesonrequest/AOR-SNCY2MCWSIK7JBSECBKH.
Type	article (author version)
Additional Information	There are other files related to this item in HUSCAP. Check the above URL.
File Information	Macromolecules(2022)_Li .pdf

Instructions for use

Effect of salt on dynamic mechanical behaviors of polyampholyte hydrogels

Xueyu Li[1,#], Feng Luo[1,2,#,], Tao Lin Sun[1,3], Kunpeng Cui[4,5], Reina Watanabe[6], Tasuku Nakajima[1,4], and Jian Ping Gong[1,4,*]*

[1]Laboratory of Soft & Wet Matter, Faculty of Advanced Life Science, Hokkaido University, Kita 21, Nishi 11, Kita-ku, Sapporo 001-0021, Japan

[2]College of Polymer Science and Engineering, State Key Laboratory of Polymer Materials Engineering, Sichuan University, Chengdu 610065, China

[3]South China Advanced Institute for Soft Matter Science and Technology, South China University of Technology, Guangzhou 510640, China

[4]Institute for Chemical Reaction Design and Discovery (WPI-ICReDD), Hokkaido University, Kita 21, Nishi 11, Kita-ku, Sapporo 001-0021, Japan

[5]Department of Polymer Science and Engineering, University of Science and Technology of China, Hefei 230026, China

[6]Laboratory of Soft & Wet Matter, Division of Soft Matter, Graduate School of Life Science, Kita10, Nishi 8, Kita-ku, Sapporo, Hokkaido 060-0810, Japan

Table of Contents

TSS (time-salt superposition): $E \rightarrow Q_V E, \quad C_{\text{NaCl}} \rightarrow a_{salt}\dot{\varepsilon}\tau_c$
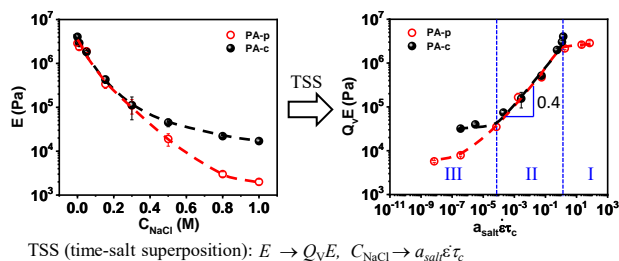
For Table of Contents use only

ABSTRACT

Understanding the dynamic mechanical behaviors of tough hydrogels with ionic dynamic bonds in saline solution is crucial for applications, particularly in the biomedical field. In this work, using polyampholyte hydrogels, dually crosslinked with a primary network from covalent crosslinkers and/or trapped entanglements, and a dynamic network from ionic bonds, as a model system, we investigate the salt effect on rheological response and mechanical behaviors. Through a systematic study on one gel without chemical crosslinker and one gel with chemical crosslinker, we demonstrate that the salt effect on mechanical properties, including small-strain moduli, large deformation energy dissipation, and fracture stretch ratio, can be effectively converted into frequency or strain rate dependences, following the time-salt superposition principle. Accordingly, we access a wide range of observation time scale from 10^{-11} to 10^2 rad/s at room temperature, covering three regimes: (I) the high-frequency plateau regime from the dynamic and primary networks, (II) the viscoelastic regime from Sticky Rouse motion of ionic associations, and (III) the low-frequency plateau regime from the primary network. Moreover, we disclose an in-depth understanding of the entanglement's behavior in the long-timescale regime III. This work not only provides a guide to biological applications of hydrogels in saline environments, but also gives

important insight into toughening mechanism via dynamic bonds in other systems with dually crosslinked structures.

KEYWORDS

Self-healing hydrogels, Dynamic bonds, Time-salt superposition, Mechanical property, Dynamic behavior, Entanglement

INTRODUCTION

Creating mechanically robust and tough hydrogels has flourished over the past two decades,[1-7] which has enabled the practical application of hydrogels in various fields requiring load-bearing, such as scaffolds for tissue engineering,[8-10] medical implants,[11] wound dressings,[12-13] flexible and wearable devices,[14-16] etc. The basic principle for developing tough hydrogels is incorporating built-in energy dissipation mechanisms through covalent/noncovalent bonds as sacrificial bonds.[17-18] Recently, incorporating dynamic noncovalent bonds into hydrogels as reversible sacrificial bonds have attracted extensive attention since the dynamic bonds not only endow hydrogels with high toughness but also self-healing ability.[19-20] Hydrogels with ionic bonds, such as polyampholyte hydrogels (PA gels),[21-23] polyion-complex hydrogels (PIC gels),[24-25] and polyelectrolytes complexed with multivalent ionic groups,[26-28] are a typical representative of hydrogels with dynamic noncovalent bonds. Among them, the PA gels consisting of polymer networks bearing randomly dispersed cationic and anionic repeat groups, exhibit tunable multiple mechanical properties over wide ranges. The tough PA gels form around the charge balance point at high concentration, as a result of randomness of opposite charges forming multiple ionic bonds with a wide distribution of strengths, through inter and intrachain complexation.[21] Therefore, they

exhibit strong viscoelasticity[29-31] and 100% self-recovery.[22] In addition, PA gels prepared at high monomer concentrations have a high toughness comparable to skeletal muscle[32-34] and excellent fatigue resistance.[35-37] Moreover, they exhibit excellent biocompatibility,[38] biological adhesion,[39-40] and anti-biofouling properties,[21] possessing great potential as structural biomaterials.

Typically, PA gels have a hierarchical structure, consisting of a transient network at the ~1 nm scale by the reversible ionic bonds, a primary polymer network at the 10 nm scale by chemical crosslinking and/or trapped entanglement, and a bicontinuous phase network at the 100 nm scale that strongly depends on the strength of ionic bonds and molecular weight between the effective crosslinking points (M_{eff}).[41] The hierarchical structure endows PA gels with a multiscale fracture process, responsible for the large energy dissipation and crack resistance, which substantially enhances the toughness and anti-fatigue.[32, 35-36] Specifically, the reversible ionic bonds not only contribute to substantial energy dissipation in large deformation but also protect the permanent bonds from breaking due to rapid self-healing in fatigue test.[37]

While the ionic bonds play a crucial role in forming hierarchical structures and realizing glamorous mechanical performance in PA gels, they become destabilized in the presence of salt since the strength of the charge attraction is screened by small ions in the system. The screening effect of salt accelerates the dissociation process of ionic bonds in PA gels,[37, 42] weakening the ionic bonds between opposite charges on the polymer chains. As a result, the PA gels, having a polymer volume fraction of 45 vol% in water, swell in saline solution of high ionic strength and soften.[43-44] Studying the effect of the saline solution on PA gels' physical and mechanical properties is important not only for understanding the role of ionic bonds but also for biological application in saline environment.

Although it has been known that salt significantly impacts the association of ionic bonds, a universal physical rule for salt effect on the dynamics and large deformation mechanical properties in hydrogels with ionic bonds as sacrificial bonds is still lacking. In this work, we systematically study rheology and large-strain mechanical behavior of hydrogels with ionic bonds as built-in energy dissipation mechanisms in saline solution, using tough and self-healing PA gels as a model system. PA gels are dually crosslinked gels with a primary network from covalent cross-linkers and/or trapped entanglements, and a dynamic network from ionic bonds. Combining rheology measurement, tensile test, and cyclic loading test, we found that the essence of salt effect is able to explained by the time-salt superposition principle no matter for the small-strain rheology or large-strain deformation, since salt accelerates the dynamics of ionic bonds, which is equivalently prolong the observation time scale for salt-free polyampholytes at room temperature. Accordingly, via addition of salt, we equivalently access a wide range of time scales to study mechanical and viscoelastic behaviors at room temperature. As a result, three frequency/strain rate regimes are accessed, including (I) the high-frequency/strain rate plateau regime from the dynamic and primary networks, (II) the viscoelastic regime from Sticky Rouse motion of ionic associations, and (III) the low-frequency/strain rate plateau regime from the primary network. Due to the limitation of observation time scale, our previous studies revealed that topological entanglement in salt-free PA gels, trapped by strong ionic bonds, plays a similar role to chemical crosslinking, [36, 41] even at a raising temperature. Thanks to the time-salt superposition, we can access a much longer timescale than the time-temperature superposition of PA gels. We have acquired a more in-depth understanding of the role of topological entanglement at the long timescale, by analyzing the plateau modulus, finite extensibility, recoverability, and reversibility of two series of PA gels: one

is PA-p without chemical crosslinker and another one is PA-c with chemical crosslinker (Figure 1).

MATERIALS AND METHODS

Materials

Anionic monomer sodium *p*-styrenesulfonate (NaSS), cationic monomer 3-(methacryloylamino)propyl-trimethylammonium chloride (MPTC), crosslinker *N,N'*-methylenebis(acrylamide) (MBAA), UV initiator *α*-ketoglutaric acid, and sodium chloride (NaCl) were purchased from Wako Pure Chemical Industries, Ltd. (Japan) and used as received. Millipore de-ionized water was used in all of the experiments.

Synthesis of polyampholyte hydrogels

Polyampholyte physical hydrogels without chemical crosslinker (PA-p) were synthesized using the one-step free radical copolymerization of the anionic monomer and the cationic monomer, according to the method described in our previous reports.[21] Briefly, a mixed aqueous solution of total monomer concentration C_m (= [NaSS] + [MPTC]) of 2.0 M with optimized molar fraction of the anionic monomer f (= [NaSS]/C_m) at 0.525, 0.1mol% UV initiator (in relative to C_m), and 0.5 M NaCl (used to control the ion strength) was injected into a reaction cell (10 cm ×10 cm) consisting of a pair of glass plates with a 1 to 2 mm silicone spacer. The polymerization was carried out in argon atmosphere in which the oxygen concentration was less than 0.1 ppm by irradiating with 365 nm UV light (light intensity ~ 4 mW/cm^2) from both sides for 8 hours. After polymerization, the as-prepared PA-p was obtained. Dialyzing the as-prepared gel in pure water for 1 week to remove the counterions Na$^+$ and Cl$^-$ (water was exchanged every day), we obtained water-equilibrated (salt-free) PA-p gel. The water-equilibrated gel shrank to ~70 vol% of its

original size due to the formation of ionic bonds between the opposite charges on the polymer network after removing the counterions, corresponding to a polymer volume fraction $\phi_0 = 0.45$.

Polyampholyte hydrogel with chemical crosslinker (PA-c) was obtained by adding 0.1 mol% MBAA as a chemical crosslinker (in relative to C_m) into the mixed aqueous solution (same formula as PA-p). The polymerization was performed by the same procedure as described for the PA-p hydrogel. After reaching the equilibrated state in water, the PA-c hydrogels also shrank to about 70 vol% of its original size and corresponds to a polymer volume fraction $\phi_0 = 0.43$.

To tune the dynamics of ionic bonds, the water-equilibrated PA-p and PA-c hydrogels were immersed in a series of NaCl solutions with different concentrations for at least 1 week to reach another equilibrium (denoted as salt-equilibrium). The molar concentrations of NaCl solutions are marked as C_{NaCl}. Specifically, gels in $C_{NaCl} = 0$ M means the water-equilibrated gels and $C_{NaCl} = 0.154$ M equals the physiological solution.

Characterization of hydrogels

Swelling measurements

The water content of water-equilibrated gels was measured by the weight change upon drying using an electronic moisture balance MOC-120H (Shimazu Co., Kyoto, Japan) that evaporates the water in the gels at 120 °C. The water content c is defined as the ratio percentage by the weight of water in gels to the total weight of the gels. The polymer volume fraction of water equilibrated gels ϕ_0 was obtained from

$$\phi_0^{-1} = 1 + (\frac{c}{1-c})\frac{\rho_p}{\rho_w}$$

where the ρ_p (≈ 1.19 g/cm^3) and ρ_w (≈ 0.998 g/cm^3) were the density of dry PA[29] and water, respectively. $\phi_0 = 0.45$ and 0.43 for PA-p and PA-c, respectively.

The swelling behaviors of hydrogels in various concentrations of NaCl aqueous solutions were characterized by the volume ratio $Q_v = \lambda_s^3$, where λ_s is the length swelling ratio of salt-equilibrated hydrogels relative to the pristine water-equilibrium hydrogels. The polymer volume fractions of salt-equilibrated gels are obtained from $\phi = \phi_0/Q_v$.

Tensile test

The tensile test was carried out on dumbbell-shaped samples with the standard JIS-K6251-7 size (35 mm (L) × 2 mm (W) × 0.85–2 mm (t)) using a commercial tensile tester (Tensilon RTC-1310A, Orientec Co.). The initial standard distance L_0 between the two clamps of the tester was 12 mm and the tensile deformation was performed under an initial strain rate $\dot{\varepsilon} = 0.14$ s^{-1}. The nominal stress σ was estimated from the stretch force divided by the cross-section area of the undeformed sample. The stretch ratio λ was estimated from the clamp distance divided by L_0. The Young's modulus E was estimated as the slope of the stress-stretch ratio curve within a stretch ratio range of $\lambda = 1.03$–1.1. The values of all the mechanical properties were calculated as averages for at least three specimens. For hysteresis test, the sample was loaded to predefined stretch ratio and immediately unloaded to stretch ratio $\lambda = 1$. Both loading and unloading strain rates were $\dot{\varepsilon} = 0.14$ s^{-1}. The hysteresis energy density (U_{hys}) was estimated from the area of hysteresis loop consisted of loading and unloading curves. All measurements were performed in a bath with corresponding salt solution at 25 °C.

Rheological test

Rheological tests were performed using an ARES rheometer (advanced rheometric expansion system, Rheometric Scientific Inc.). A rheological frequency sweep from 0.0628 to 100 rad/s was performed with a shear strain of 0.1% in the parallel-plates geometry at 25 °C. The disc-shaped

samples with thicknesses of ~ 1.5 mm and diameters of 15 mm were adhered to the plates with glue and surrounded by corresponding salt solution.

RESULTS AND DISCUSSION

Swelling in saline solution

To investigate the effect of salt on the fast dynamics from dynamic network and slow dynamics from primary network, we prepared PA gels with 0 % and 0.1 mol% (relative to total monomer concentration C_m = 2.0 M) chemical crosslinkers, denoted PA-p and PA-c, respectively. Both topological entanglements and chemical crosslinking contribute to crosslink points of the primary network in water-equilibrated PA-c, while only topological entanglements contribute to crosslink points of the primary network in water-equilibrated PA-p. Left illustration in **Figure 1** shows the dually crosslinked structure of water-equilibrated PA gels, containing a primary network from covalent cross-linkers and/or trapped entanglements, and a dynamic network from ionic bonds between opposite charges on the polymer chains. To tune the association strength of ionic bonds on polymer networks, we immersed the water-equilibrated gels into NaCl solution with varied concentrations C_{NaCl} to reach a new equilibrium, denoted as salt-equilibrium. Because salt ions screen the Coulomb interaction between charged groups,[45] the ionic bonds strength is weakened. As a result, the PA gels swell by a length swelling ratio $\lambda_s > 1$ (right of **Figure 1**). In the following sections, we will study the salt effect on swelling, rheological response, large deformation, and energy dissipation to understand the underlying toughening mechanism of ionic bonds.
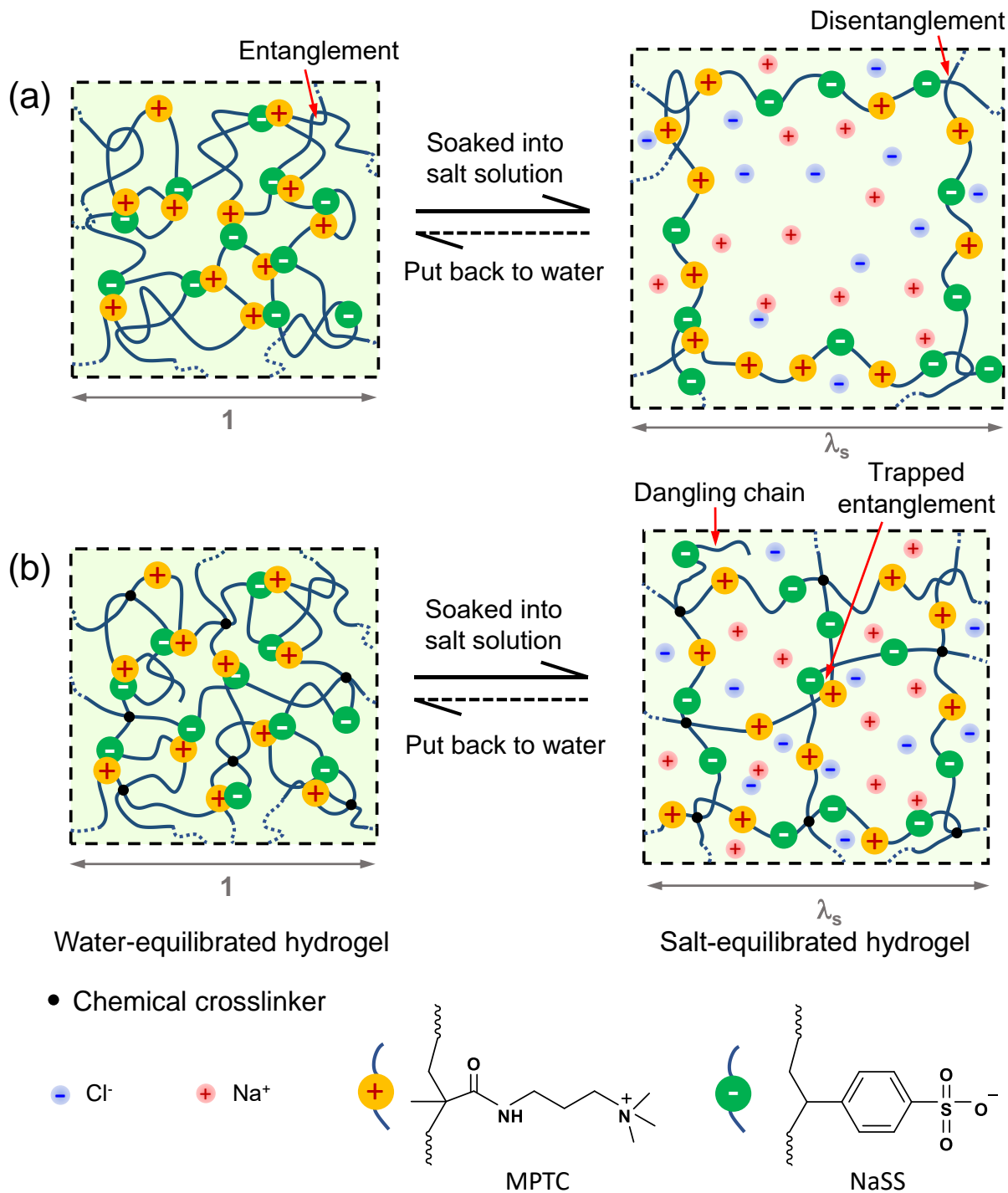
Figure 1. Illustration of salt effect on the dually crosslinked networks in polyampholyte (PA) gels without (PA-p) and with (PA-c) chemical crosslinking. (**a**) The water-equilibrated (salt-free) PA-p composed of a primary network from topological entanglements, and a dynamic network from ionic bonds between charged groups (left). After immersing in NaCl solutions ($C_{NaCl} \leq 1.0$ M) to reach salt equilibrium, the PA-p swells as salt ions screen the Coulomb interaction between charged groups and the strength of ionic association weakens (right). At high C_{NaCl},

disentanglement occurs, resulting in irreversible change of the dually crosslinked networks. (**b**) The water-equilibrated (salt-free) PA-c composed of a primary network from chemical crosslinking and trapped topological entanglements, and a dynamic network from ionic bonds (left). After immersing in NaCl solutions, the PA-c also swells (right). The water-equilibrated gels are taken as reference state (length swelling ratio = 1), and the salt-equilibrated hydrogels have a length swelling ratio λ_s.

Figures 2a and **2b** show the optical images at different C_{NaCl} for PA-p and PA-c, respectively. The transparency decreases with C_{NaCl}, indicating that salt ions lead to a more heterogeneous structure. As revealed in our previous work,[41] the characteristic length of the phase-separated network in water-equilibrated PA-c is much smaller than the water-equilibrated PA-p, thus the PA-c is more transparent than PA-p at the same salt condition. The C_{NaCl} dependence of swelling volume ratio Q_v or polymer volume fraction ϕ ($=\phi_0/Q_v$) for PA-c is weaker than that of PA-p (**Figure 2c**), since PA-c is permanently crosslinked by chemical crosslinkers against the swelling due to disassociation of ionic bonds.
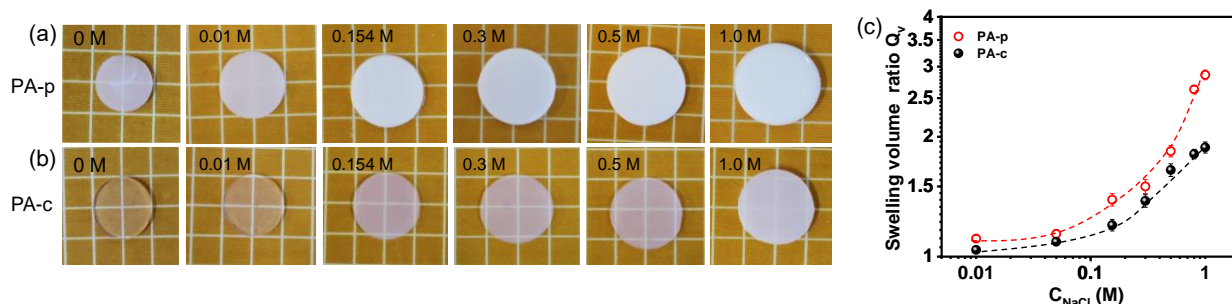

Figure 2. Effect of salt concentration (C_{NaCl}) on the appearance and swelling of the equilibrated PA gels: PA-p without chemical crosslinker and PA-c with 0.1 mol% chemical crosslinker. (**a**-**b**) Appearance of PA-p (a) and PA-c (b) gels in varied C_{NaCl} from $C_{NaCl} = 0$ to 1.0 M. The mesh size of the background lattice is 5 mm. (**c**) Swelling volume ratio relative to water-equilibrated gels (Q_v) as a function of C_{NaCl}.

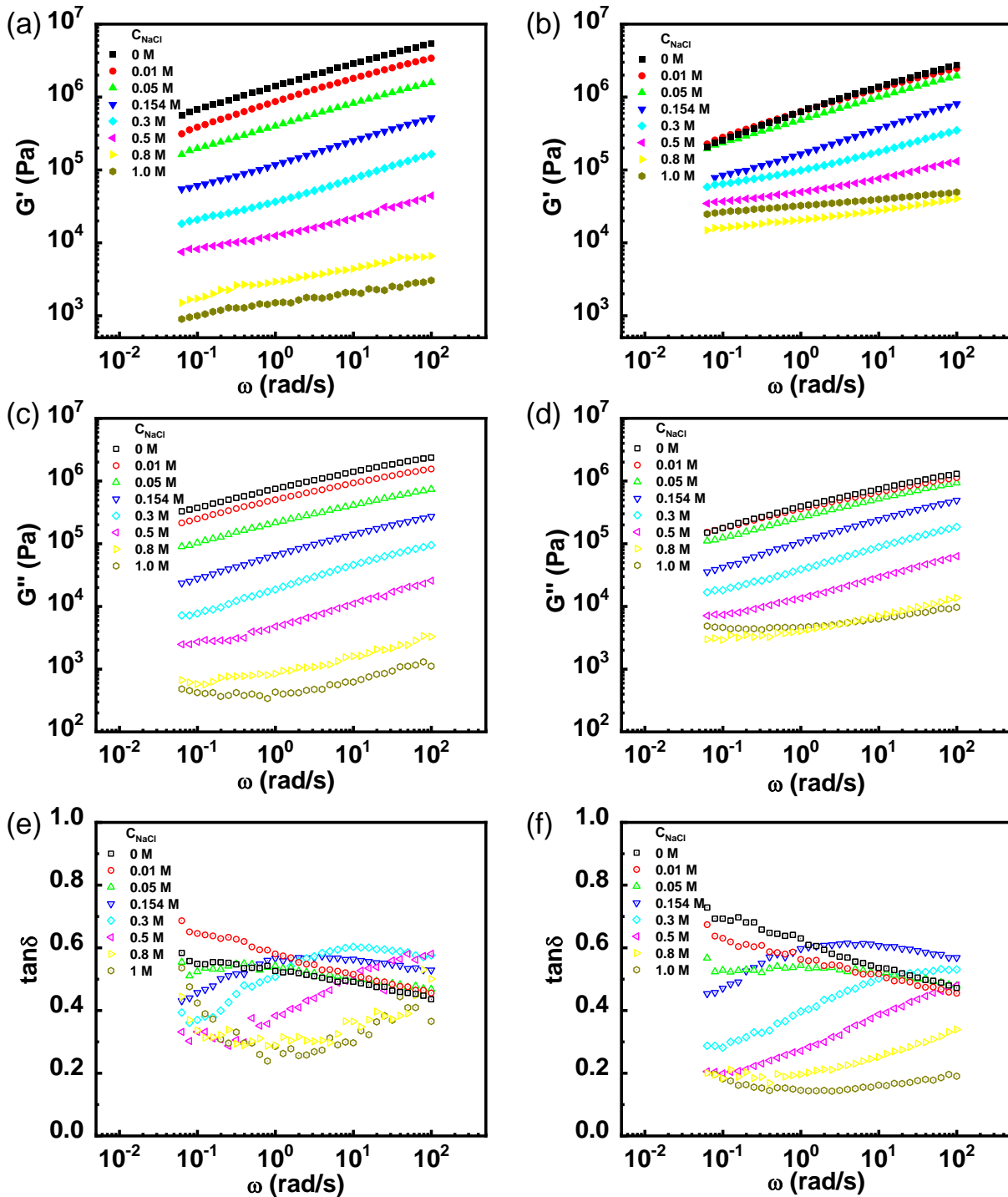**Time-salt superposition for linear dynamic mechanical behavior**

Figure 3. Dynamic mechanical behavior of PA-p and PA-c equilibrated in varied salt concentration C_{NaCl} at 25 °C. The frequency sweep curves of (**a**) storage modulus G' (**c**) loss modulus G'', and (**e**) loss factor tanδ for PA-p, (**b**) G' (**d**) G'', and (**f**) tanδ for PA-c in C_{NaCl} from 0 to 1.0 M.

Figure 3 shows the linear dynamic mechanical behavior of PA gels in varied saline solutions at angular frequency $\omega = 0.0628$ to 100 rad/s. Due to weakening of ionic bonds strength, the storage and loss moduli decreases with increasing C_{NaCl}. Spruijt et al.[42] reported salt concentration plays a similar role as strain rate, and revealed time-salt superposition principle in polyelectrolyte complexes. In our recent work,[37] we also demonstrated that the salt-containing and salt-free PA gels obey time-salt superposition principle, since salt accelerates the dissociation processes of ionic bonds, which is equivalent to prolong the observation time scale for salt-free samples. That is the dynamic mechanical behavior (the log-log $G(\omega)$–frequency curves) of salt-containing gels $G_{salt}(\omega)$ overlap on the $G(\omega)$ curve of salt-free PA gels, by using proper horizontal shift factor a_{salt} and vertical shift factor $b_{salt} = Q_v$, where the a_{salt} is determined by superimposing the $G_{salt}(\omega)$ curve on the $G(\omega)$ curve of salt-free PA gels. $b_{salt} = Q_v = \lambda_s{}^3$ is due to overall polymer density difference per volume. Here, we take the gels in $C_{NaCl} = 0$ as reference state, and the frequency of salt-containing gels shift to be $a_{salt}\omega$. As expected, **Figures 4a,4b** shows that the Q_vG' and Q_vG'' overlap on master curves at $C_{NaCl} \leq 0.5$ M and $C_{NaCl} \leq 0.8$ M for PA-p and PA-c, respectively. The loss factor tanδ just roughly overlap on the master curves due to deviation from both Q_vG' and Q_vG''. In the viscoelastic regime, the Q_vG' on the master curve increases with $a_{salt}\omega$, and follows $Q_vG' \sim (a_{salt}\omega)^\beta$. This can be attributed to the Sticky Rouse motion of associating polymer strands derived from ionic bonds (sticker).[46] Normally, β has a value of $\beta = 0.5$. But here the β is smaller than 0.5 ($\beta \approx 0.35$), probably due to a distribution in strength of ionic bonds in PA gel, as seen by the heterogeneous structure.[47] Further increasing the C_{NaCl} to $C_{NaCl} > 0.5$ M and $C_{NaCl} > 0.8$ M for PA-p and PA-c, respectively, the Q_vG'' and tanδ increase with decreasing frequency below a turning point at low frequency limit, indicating Rouse motions of the whole entangled/crosslinked polymer chains.[48]

The horizontal shift factor a_{salt}, related to relaxation dynamics of ionic association in varied C_{NaCl} is shown in **Figure 4c**. Here, the Arrhenius equation [49] may be written to be $a_{\text{salt}} = A\exp[E_a(C_{\text{NaCl}})/RT]$, where $E_a(C_{\text{NaCl}})$ is the apparent activation energy for ionic bonds dissociation in C_{NaCl}, R is the ideal gas constant, T is absolute temperature, and A is a constant. PA-p shows smaller a_{salt} than PA-c at the same C_{NaCl}, probably because a stronger C_{NaCl} dependence of $E_a(C_{\text{NaCl}})$ in PA-p than in PA-c. The weaker C_{NaCl} dependence of $E_a(C_{\text{NaCl}})$ in PA-c could be understood by a higher barrier by chemical crosslinking against dissociation. Intriguingly, the a_{salt} is inversely correlated to the swelling ratio Q_v, as seen from the overlap of a_{salt} versus Q_v plot for PA-p and PA-c (**Figure 4d**). The $E_a(C_{\text{NaCl}})$ is the energy barrier for ionic bonds dissociation, which should be positively related the Coulomb attraction E_{coulomb} between opposite charges on polymer strands, $E_a(C_{\text{NaCl}}) \propto E_{\text{coulomb}} \sim q_1 q_2/\varepsilon r$, where q_1 and q_2 are electric charge of cation and anion, respectively. ε is the dielectric constant, and r is the distance between the cation and anion on the interacting polymer strands. With increase of Q_v, the distance between polymer strands increases, results in a larger r and thus a smaller E_{coulomb} and $E_a(C_{\text{NaCl}})$. Therefore, the a_{salt} is inversely correlated to Q_v.

Overall, **Figure 4** shows that the effect of salt on the dynamic mechanical behaviors of both PA-p and PA-c obeys time-salt superposition principle over a board range of salt concentrations. Salt effect is equivalent to prolonging the observation time scale of the water-equilibrated gels, therefore, the dynamic mechanical behavior of water-equilibrated gels can be accessed over a wide frequency range (10^{-11} to 10^2 rad/s for PA-p and 10^{-8} to 10^2 rad/s for PA-c) by measurement at room temperature in varied salt concentrations. The Q_vG' for both PA-p and PA-c does not reach the plateau modulus at the high-frequency limit, indicating that the lifetimes of the associations (τ_s) are short, beyond our observation window ($\tau_s < 10^{-2}$ s) in room temperature. Hereafter, we use angular frequency ω_c at the peaks of tanδ to denote the main viscoelastic relaxation from the Rouse

motion of associating strands in salt-free PA gels. From the viscoelastic peaks of tanδ at $\omega_c = 0.002$ and 0.1 rad/s, we get viscoelastic relaxation times of $\tau_c = 1/\omega_c = 500$ and 10 s for salt-free PA-p and PA-c, respectively. The reason for PA-p showing a larger τ_c than PA-c may derive from the larger M_{eff}, which delays the Rouse time of polymer strands.
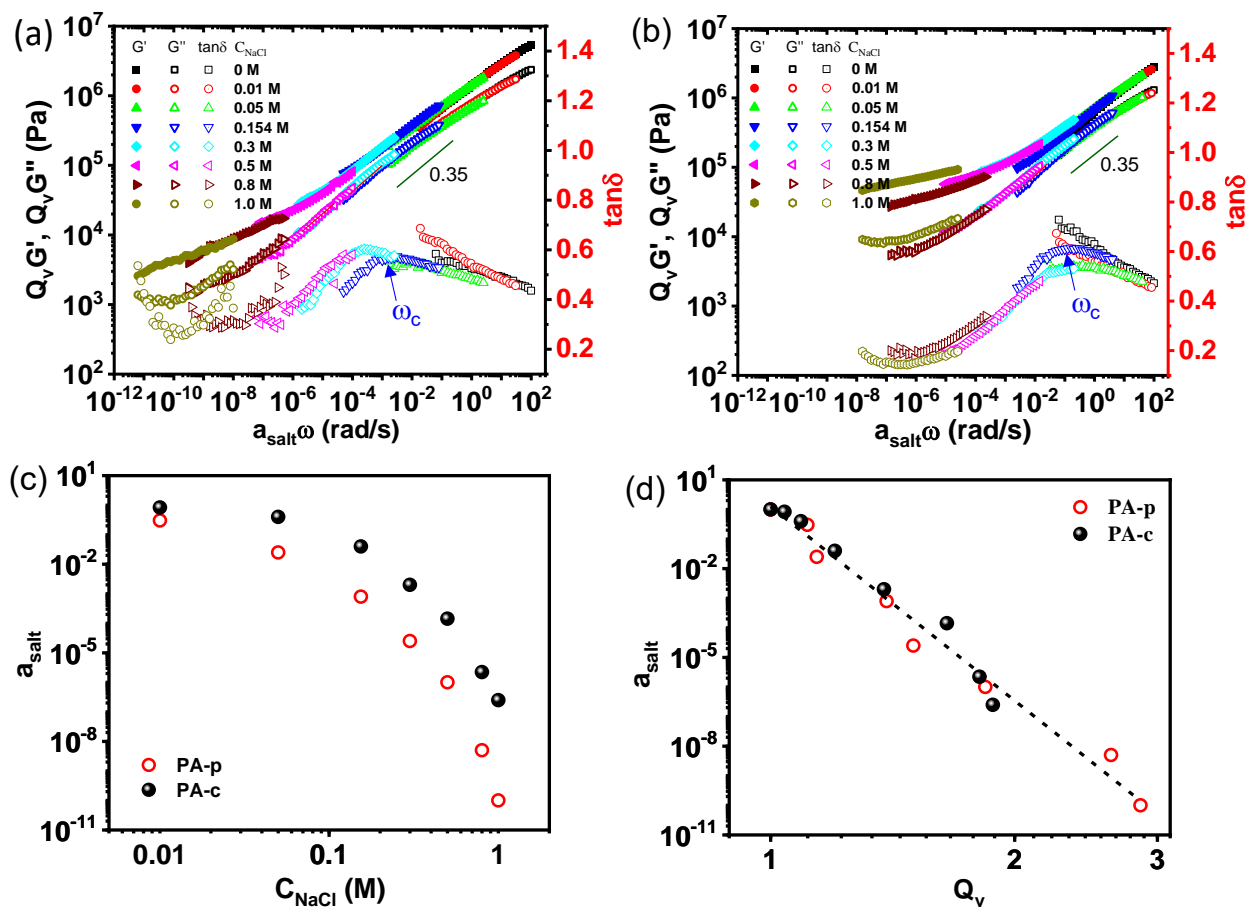

Figure 4. Constructed master curves of linear dynamic mechanical behavior of equilibrated PA gels through time–salt superposition. (**a**–**b**) The master curves of storage modulus G', loss modulus G'', and loss factor tanδ constructed from time–salt superposition for (a) PA-p and (b) PA-c using data in **Figure 3**. The water-equilibrated gels ($C_{NaCl} = 0$) are taken as a reference state. (**c-d**) The time−salt superposition's horizontal shift factor a_{salt} as a function of C_{NaCl} (c) and corresponding Q_v (d). The vertical shift factor in (a, b) is volume swelling ratio Q_v. The dashed line in (d) is a guide for the eyes.

Using the obtained master curve, we estimate the number of monomer units per network strands $N_{x,eff}$ of the PA gels from the shear modulus $Q_v G'$ in the quasi-plateau regime at low frequency, where the contribution of ionic bonds is negligible, using the relation

$$Q_v G' = \frac{\rho \phi_0 N_A k_B T}{M_0 N_{x,eff}}$$
(1)

ρ is dry polymer density (1.19 g/cm^3).[29] k_B and T are Boltzmann constant (1.38×10^{-23} J/K) and the absolute temperature (297.15 K), respectively. M_0 and N_A are the average molecular weight of the monomers (213.5 g/mol) and Avogadro constant (6.02×10^{23} /mol), respectively. For PA-c, the $Q_v G' = 26.9$ kPa was taken from the quasi-plateau at low frequency (corresponding to $C_{NaCl} = 0.8$ M, $a_{salt}\omega = 10^{-7}$ rad/s) of the master curve in **Figure 4b**. For PA-p, we took the corresponding $Q_v G'$ = 6.8 kPa at the frequency of turning point of tanδ at the low-frequency limit (corresponding to $C_{NaCl} = 0.8$ M, $a_{salt}\omega = 10^{-8}$ rad/s) in **Figure 4a**. The reason to choose this turning point is that Rouse motions of the whole entangled polymer chains occur below the frequency of this point, as suggested in **Figure 4a**. Substituting the $Q_v G'$ values, we get $N_{x,eff} = 830$ and 210 for PA-p and PA-c, respectively. Given that both the chemical crosslinker and trapped entanglement have four functionalities,

$$N_{x,eff} = 1/[2(\nu_x + \nu_e)]$$
(2)

Here, ν_x and ν_e are the number densities of chemical crosslinking and trapped topological entanglements (mol% in relative to monomer units), respectively. Assuming that the chemical crosslinking reaction efficiency is ~100%, then $\nu_x = C_{MBAA} = 0.1$ mol% = 0.001, we have ν_e = 0.0014 = 0.14 mol% for PA-c. For PA-p, since $\nu_x = 0$, we have $\nu_e = 6.0 \times 10^{-4} = 0.06$ mol%. The number density of topological entanglements ν_e is related to the monomer concentration at preparation (C_m) by $\nu_e \approx \alpha C_m^{2.3}$,[48] where $\alpha = 0.031$ mol%·M$^{-2.3}$ based on our previous fitting result

of PA gels.[41] For the samples used in this work, $C_m = 2.0$ M, which gives $\nu_e = 0.15$ mol%. The ν_e

estimated for PA-c (0.14 mol%) is consistent with this value while ν_e estimated for PA-p (0.06

mol%) is much smaller. This indicates that at the high salt concentration of $C_{NaCl} = 0.8$ M, the

entanglements trapped by chemical crosslinking in PA-c cannot disentangle. In contrast, the

entanglements in PA-p mainly stabilized by ionic bonds[29] relax at $1/\omega = 3$ s in $C_{NaCl} = 0.8$ M

(equivalent to prolong the observation time scale to $1/(a_{salt}\omega) \sim 10^8$ s in water). It should be

mentioned that, the PA-p can completely dissolve into higher salt concentration, such as in C_{NaCl}

$= 4$ M (**Figure S1**). In this case, the disentanglement (or chain reptation) occurs more rapidly than

in $C_{NaCl} = 0.8$ M.

At a low salt concentration (corresponding to observation at high frequency), the PA-p could

not disentangle in the observation time scale due to the existence of strong ionic bonds which

stabilize the entanglements.[29] To find the critical frequency for PA-p start to disentangle, using ν_e

$= 0.15$ mol%, we get $N_{x,eff} = 330$ and $Q_v G' = 18.7$ kPa, which corresponds to $\omega = 0.3$ rad/s in C_{NaCl}

$= 0.5$ M, and $a_{salt}\omega = 3.2 \times 10^{-7}$ rad/s on the master curve of salt-free gel.

Time-salt superposition for large-strain mechanical behavior

From above small-strain rheology results we known that the salt effect is essentially a change

in relative frequency/strain rate, following time-salt superposition. How about the salt effect on

large deformation? We performed tensile test for PA gels in varied C_{NaCl}, under an initial strain

rate $\dot{\varepsilon} = v/L_0 = 0.14$ s^{-1}, where v is the loading speed (100 mm/min) and L_0 (12 mm) is the gauge

length of precut dumbbell specimens. The tensile behavior of water-equilibrated ($C_{NaCl} = 0$ M) and

salt-equilibrated ($C_{NaCl} > 0$ M) PA gels is shown in **Figure 5**. Stress falls with C_{NaCl} due to the

screening of interchain ionic bonds. The fracture stretch ratio (λ_b) of PA-p starts to increase

obviously at $C_{NaCl} = 0.5$ M, and it increases two times at $C_{NaCl} = 0.8$ and 1.0 M with dramatic

stress-weakening (**Figures 5a,5d**). In contrast, the λ_b of the PA-c only shows about 40% increase at high C_{NaCl} (**Figures 5b,5d**).

Owing to screening of interchain ionic bonds, **Figure 5c** shows that the Young's modulus (E) decreases with C_{NaCl}. Particularly, the E of PA-p and PA-c are almost the same at $C_{NaCl} < 0.5$ M, while further increasing C_{NaCl}, E of PA-p decreases more than PA-c. The results suggest that the E is dominated by ionic bonds in low salt concentration whereas disentanglement of polymer chains in PA-p occurs at high salt concentration. Since E is also a quantity of small deformation, it should show similar behavior as G'. To confirm this, the salt effect on E is converted to strain rate dependence through the time-salt superposition introduced in the above rheology result. We rescale the E as $Q_v E$ to normalize the strand density per unit volume taking the gels in $C_{NaCl} = 0$ M as a reference state. As the salt accelerates the dissociation processes of ionic bonds by a factor of a_{salt}, we use the product of a_{salt} in rheological test and strain rate $\dot{\varepsilon}$ to denote the equivalent strain rate ($a_{salt}\dot{\varepsilon}$) in tensile test at the reference state (salt free state). In order to compare the tensile results with the rheological results, we need to correlate the equivalent strain rate ($a_{salt}\dot{\varepsilon}$) with the angular frequency ($a_{salt}\omega$). A quantitative comparison between the dynamic behaviors measured by rheology test and the tensile test of a viscoelastic material is inherently limited due to the continuous changes in velocity during the oscillation in the rheology test. Here, we compared the Young's modulus $Q_v E$ from the uniaxial tensile test with the norm of complex modulus $Q_v |G^*|$ from the rheology test. The relation $E=3|G^*|$ holds for incompressible materials. We found that the plot of $Q_v E$ vs $2\pi a_{salt}\dot{\varepsilon}$ agrees with the plot of $3Q_v|G^*|$ vs $a_{salt}\omega$, suggesting $\omega=2\pi\dot{\varepsilon}$ (**Figure S2**). Hereafter, we use $\omega=2\pi\dot{\varepsilon}$ to compare the dynamic behaviors measured by rheology test and the tensile test. Therefore, the dimensionless quantity, $2\pi a_{salt}\dot{\varepsilon}\tau_c$, denotes the equivalent strain rate ($a_{salt}\dot{\varepsilon}$) relative to the main viscoelastic relaxation rate ($\tau_c = 1/\omega_c$). For the sake of simplicity, we

use $a_{salt}\dot{\varepsilon}\tau_c$ to denote the relative equivalent strain rate in the following section, and the constant 2π will be introduced when we compare the strain rate–dependence in tensile test with the angular frequency–dependence of rheology test.

Figure 5e shows the Q_vE versus $a_{salt}\dot{\varepsilon}\tau_c$ plot. The master curve shows three strain rate regimes. (I) At $a_{salt}\dot{\varepsilon}\tau_c > 1$, Q_vE is weakly rate dependence. Since $a_{salt}\dot{\varepsilon}\tau_c > 1$ denotes the strain rate larger than the 2π times of main viscoelastic relaxation rate, almost all the ionic bonds act as stickers and contribute to the modulus. (II) At $7\times10^{-5} < a_{salt}\dot{\varepsilon}\tau_c < 1$, Q_vE increases with $a_{salt}\dot{\varepsilon}\tau_c$ following a power law $Q_vE \sim (a_{salt}\dot{\varepsilon}\tau_c)^{0.4}$ for both PA-p and PA-c, indicating viscoelastic behavior, which correlated to the break-up of stickers. This scaling exponent is consistent with the previously reported value of testing a water-equilibrated PA gel in a strain rate regime of 10^{-3} to 1 s^{-1} ($E \sim \dot{\varepsilon}^{0.41}$).[34] (III) At $a_{salt}\dot{\varepsilon}\tau_c < 7\times10^{-5}$, PA-c shows weak rate dependence again. At this regime, the effect of ionic bonds almost disappears, and the moduli only correlated to the chemical crosslinker and trapped entanglements.[29] But the Q_vE of PA-p further decreases to a small value of 7.89 kPa, and show weak rate dependence until $a_{salt}\dot{\varepsilon}\tau_c < 10^{-6}$. Substituting $3G' = Q_vE = 7.89$ kPa (assuming incompressible materials) to eqs. 1 and 2, we get $N_{x,eff} = 2.35\times10^3$ and $C_e = 0.02$ mol%. The latter is much smaller than the theoretically value $C_e = 0.15$ mol%, indicating the occurrence of disentanglement in PA-p in the regime III. This coincides with our rheology test (**Figure 4a**), that the disentanglement occurs at $a_{salt}\omega < 3.2\times10^{-7}$ rad/s, corresponding to $a_{salt}\dot{\varepsilon}\tau_c = a_{salt}\omega\tau_c/2\pi < 2.5\times10^{-5}$.
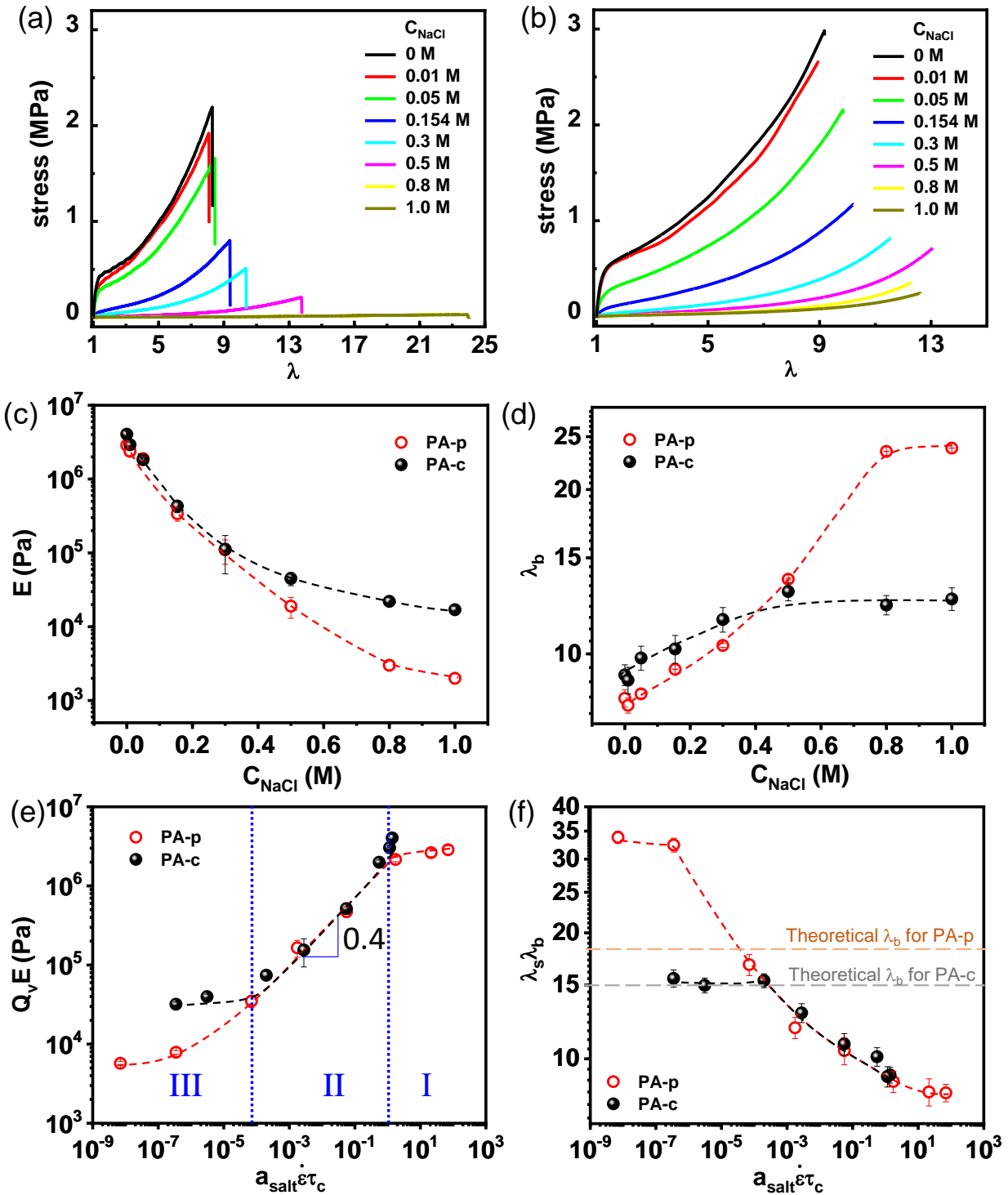
Figure 5. Time-salt superposition for tensile test. (**a-b**) Stress-stretch ratio (λ) curves of equilibrated PA-p (a) and PA-c (b) in varied C_{NaCl}. The stress is force over the initial undeformed cross-sectional area, $λ$ is the ratio between clamp distance and the initial gauge length. (**c-d**) The

Young's modulus E (c) and fracture stretch ratio λ_b (d) as a function of C_{NaCl}. (**e-f**) Time-salt superposition of the rescaled Young's modulus Q_vE (e) and fracture stretch ratio $\lambda_s\lambda_b$ (f). The dotted blue vertical lines in (e) mark the boundaries between three strain rate regimes. The strain rate is denoted by a dimensionless quantity, $a_{salt}\dot{\varepsilon}\tau_c$, denoting the equivalent strain rate in relative to the main viscoelastic relaxation rate of the water-equilibrated gels. The dashed lines are a guide for the eyes.

The salt effect on the fracture stretch ratio of PA gels is also convert to strain rate dependence through the time-salt superposition. The facture stretch ratio λ_b is rescaled by the swelling ratio (λ_s) in length as $\lambda_s\lambda_b$. **Figure 5f** shows that the $\lambda_s\lambda_b$ versus $a_{salt}\dot{\varepsilon}\tau_c$ curves of for PA-p and PA-c overlap on a master curve at $a_{salt}\dot{\varepsilon}\tau_c > 7\times10^{-5}$, and $\lambda_s\lambda_b$ decreases with increasing $a_{salt}\dot{\varepsilon}\tau_c$. This is because more ionic bonds act as effective crosslinkers/stickers at larger $a_{salt}\dot{\varepsilon}\tau_c$, which limits the extensibility. At $a_{salt}\dot{\varepsilon}\tau_c < 7\times10^{-5}$, $\lambda_s\lambda_b$ of PA-c reaches a plateau. In contrast, $\lambda_s\lambda_b$ of PA-p further increases to a larger value with decreasing $a_{salt}\dot{\varepsilon}\tau_c$. To find the physical meaning of this phenomenon, we calculated the theoretical fracture ratio $\lambda_b^{theory} = N_{x,eff}b/(\xi/\lambda_s)$ from the ratio of chain contour length $N_{x,eff}b$ and the end-to-end distance of the network strand (ξ) in salt but normalized to water-equilibrated state (ξ/λ_s). The b is monomer length, and $\xi/\lambda_s = bN_{x,eff}^{1/2}$ assuming that the network strands are ideal coil. Note that, for water-equilibrated gels, the scaling exponent of ξ and $N_{x,eff}$ should be $\xi = bN_{x,eff}^{1/3}$, since the strands are in their collapsed globule conformation due to the interaction between the opposite charges on the chains.[36, 50] But here, in high concentration salt solution, given little contribution from ionic bonds, we hypothesized that the chain strands are ideal coils at the reference state. Then, we get the theoretical fracture stretch ratio $\lambda_b^{theory} = N_{x,eff}^{1/2}$. Substituting $N_{x,eff} = 333$ (from 0.15 mol% topological entanglement) and 210 (from 0.1 mol% chemical crosslinking and 0.14% topological entanglement), we get $\lambda_b^{theory} = 18$ and 15 for PA-p and PA-c, respectively. **Figure 5f** shows that PA-c has a $\lambda_s\lambda_b \approx 15$ at $a_{salt}\dot{\varepsilon}\tau_c < 7\times10^{-5}$ where the viscoelasticity becomes very weak. This suggests that the $\lambda_s\lambda_b$ at the low strain

rate regime results from finite extensibility of polymer strands crosslinked by the chemical crosslinker and trapped entanglements, not by the ionic bonds. In contrast, the $\lambda_s\lambda_b = 32$ of PA-p is much higher than 18 at $a_{salt}\dot{\varepsilon}\tau_c < 7\times10^{-5}$, suggesting the occurrence of disentanglement and pull-out of chains in large deformation.

The effect of salt on bulk energy dissipation at large strain is investigated by cyclic tests at a large fixed peak stretch ratio $\lambda = 2$ under a nominal strain rate $\dot{\varepsilon} = 0.14$ s^{-1}. As shown in **Figure 6a**, large hysteresis loops are observed due to the energy dissipation from ionic bonds in salt-free gels. The hysteresis area markedly decreases with increasing salt concentration, indicating that fewer ionic bonds contribute to the energy dissipation. The hysteresis energy density U_{hys} of PA-p decreases faster with C_{NaCl} than PA-c (**Figure 6c**), consistent with the change of polymer volume fraction. We plot the rescaled $Q_v U_{hys}$ as a function of $a_{salt}\dot{\varepsilon}\tau_c$ to investigate the dynamic behavior of bulk energy dissipation (**Figure 6d**). We find that both PA-p and PA-c follow time-salt superposition similar to the G' and G'' in **Figures 4a** and **4b**

$$U_{hys}(\dot{\varepsilon}\tau_c,\ C_{NaCl}) = b_{salt}U_{hys}(a_{salt}\dot{\varepsilon}\tau_c,\ C_0) \tag{3}$$

where C_0 is $C_{NaCl} = 0$ M, $b_{salt} = Q_v$ owing to volume difference. The master curve looks similar to **Figure 5e**, showing three regimes: (I) Plateau regime at $a_{salt}\dot{\varepsilon}\tau_c > 1$, corresponds to energy dissipation from stickers. (II) Viscoelastic regime at $7\times10^{-5} < a_{salt}\dot{\varepsilon}\tau_c < 1$. The $Q_v U_{hys}$ increases with $a_{salt}\dot{\varepsilon}\tau_c$, following $Q_v U_{hys} \sim (a_{salt}\dot{\varepsilon}\tau_c)^{0.38}$, consistent with our previous time-temperature superposition result ($b_T U_{hys} \sim (a_T\varepsilon)^{0.31}$),[30] where a_T and b_T are the horizontal and vertical shift factors of the time−temperature superposition. This suggests that the salt plays similar behavior as temperature. Both of them activate the breakage of ionic bonds and accelerate chain relaxation. It also indicates that the effect of salt on the linear rheology is also applicable to the bulk energy dissipation at large deformation. (III) Weak rate dependence regime at $a_{salt}\dot{\varepsilon}\tau_c < 7\times10^{-5}$,

corresponds to negligible contribution of ionic bonds. Interestingly, when the salt effect on mechanical behaviors is converted into strain rate dependence by the time-salt superposition principle, the rate-dependent energy dissipation at large deformation (**Figure 6d**) almost has the same exponential scaling as the rate-dependent Young's modulus at small deformation (**Figure 5e**) in the viscoelastic regime. It means $U_{hys}(a_{salt}\varepsilon) \propto E(a_{salt}\varepsilon)$, suggesting that the modulus at small deformation may be able to predict the bulk energy dissipation behavior at large deformation. This needs further investigation and will be presented in a separate paper.

The disentanglement of PA-p in large C_{NaCl} results in a large residual strain during cyclic load than that of PA-c (**Figure 6b**). We investigate the recoverability of ionic bonds in varied C_{NaCl} via cyclic loads. After 1 cycle loading-unloading, PA gels relax (self-recover) for different time, then reloading and record the change of hysteresis loop. **Figure 6e** shows an example for PA-p in C_{NaCl} = 0. Recovery ratio of hysteresis energy density U_t/U_o (U_t/U_o = 100% indicates 100% recovery, while U_t/U_o = 0% indicates 0% recovery) as a function of recovery time for the PA gels in several representative C_{NaCl} is plotted in **Figure 6f.** Compared with PA gels in C_{NaCl} = 0, increasing the C_{NaCl}, the time of 100% recovery becomes shorter, since salt accelerates the dynamics of ionic bonds. Intriguingly, PA-p in C_{NaCl} = 1 M shows a weak self-recovery ability of hysteresis energy, which also supports chain pull-out at large deformation in high salt concentration.
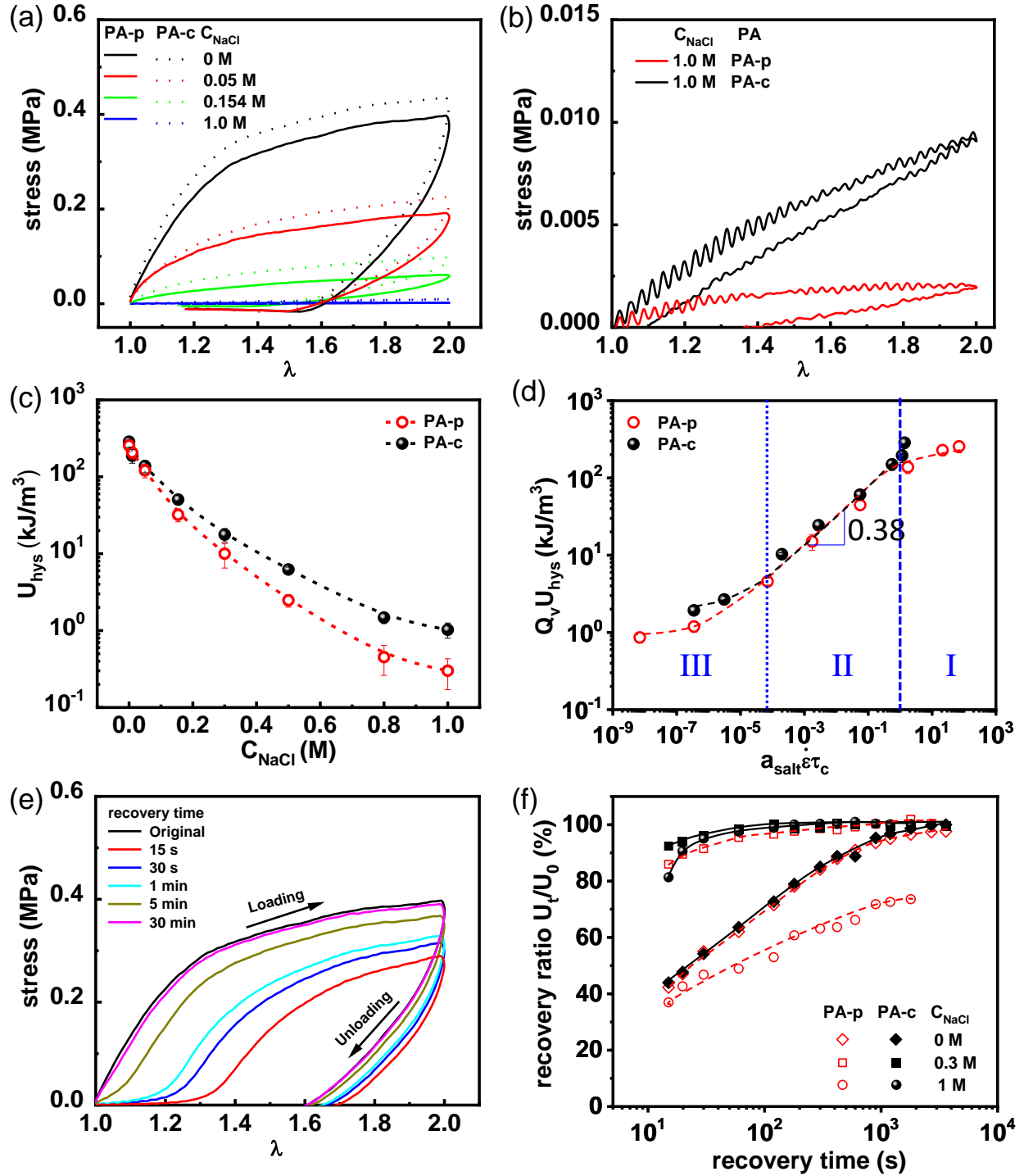
Figure 6. Cyclic tensile behavior of equilibrated PA-p and PA-c in varied C_{NaCl}. (**a**) Cyclic stress−stretch ratio (λ) curves under nominal strain rate $\dot{\varepsilon} = 0.14$ s^{-1} at room temperature. (**b**) Zoom in of stress−stretch ratio curves for PA gels in $C_{NaCl} = 1$ M. The oscillations on the stress-strain curve are from the instrument noise. (**c**) Relationship between hysteresis energy density U_{hys} and C_{NaCl}. (**d**) The master curve of rescaled hysteresis energy density $Q_v U_{hys}$ versus $a_{salt}\dot{\varepsilon}\tau_c$ plot. The dotted blue vertical lines mark the boundaries between three strain rate regimes. (**e**) Typical stress−λ curves of PA gels at different recovery time. The PA-p in $C_{NaCl} = 0$ M is taken as an

24

example. (**f**) Recovery ratio of hysteresis energy density U_t/U_0 as a function of recovery time for PA gels in varied C_{NaCl}. The dashed lines in (c) (d) and (f) are a guide for the eyes.

The reversibility of permanent and transient networks

To check whether the dually crosslinked networks are reversible or not after experiencing a disturbance of the thermodynamic environment by salt, we put the undeformed salt-equilibrated gels back into the water to dialyze the salt and get water-reequilibrated samples. The cyclic loading curves for the water-reequilibrated PA-p and PA-c are shown in **Figures 7a** and **7b**, respectively. At $C_{NaCl} < 0.3$ M, the water-reequilibrated PA-p is completely reversible in the hysteresis loop compared to the pristine salt-free gel. Whereas a dramatic increase of irreversible hysteresis is observed at $C_{NaCl} > 0.3$ M. In particular, only slight reversibility is observed for the gels treated with $C_{NaCl} = 0.8$ and 1.0 M. The PA-c shows ~100% reversibility at $C_{NaCl} < 0.8$ M, and irreversible hysteresis is observed at $C_{NaCl} = 0.8$ and 1.0 M.

To quantify the reversibility, we normalized Young's modulus (E) and hysteresis energy density (U_{hys}) of water-reequilibrated gels to E_0 and U_{hys0} of pristine salt-free gels. If the ratios E/E_0 and U_{hys}/U_{hys0} are equal to 1, it means completely reversible of the primary and transient networks; if E/E_0 and U_{hys}/U_{hys0} are smaller than 1, it means irreversible of either primary or transient networks. **Figure 7c** shows that the ratios deviate from 1 at $C_{NaCl} = 0.3$ and 0.8 M for PA-p and PA-c, respectively. As demonstrated above, disentanglement occurs at $C_{NaCl} = 0.5$ M in PA-p, slightly larger than the critical C_{NaCl} for irreversible E/E_0 and U_{hys}/U_{hys0}. It suggests that permanent damage of transient networks happens before the occurrence of disentanglement of polymer chains. As for PA-c, the critical C_{NaCl} for irreversible E/E_0 and U_{hys}/U_{hys0} is also smaller than the C_{NaCl} for G' and G'' hardly overlapping on the time−salt superposition master curve

(**Figure 4b**). This suggests that the permanent damage of transient network happens before the occurrence of the primary network damage.

We plot the E/E_0 and U_{hys}/U_{hys0} as a function of the corresponding swelling ratio Q_v in C_{NaCl} (**Figure 7d**). It shows that the plots almost overlap on a corresponding master curve. At $Q_v < 1.8$, E/E_0 and U_{hys}/U_{hys0} are close to 1 (both PA-p and PA-c), while decrease dramatically at $Q_v > 1.8$ (PA-p). For PA-p, the latter case may be caused by the disentanglement and reptation of polymer chains, which leads to remarkable irreversibility in primary network and dynamic network. We noted that the PA-c in $C_{NaCl} = 0.8$ ($Q_v = 1.81$) and 1 M ($Q_v = 1.88$) is slightly irreversible. This may be due to permanent damage of the transient network and the pull-out of dangling chains during the swelling process.
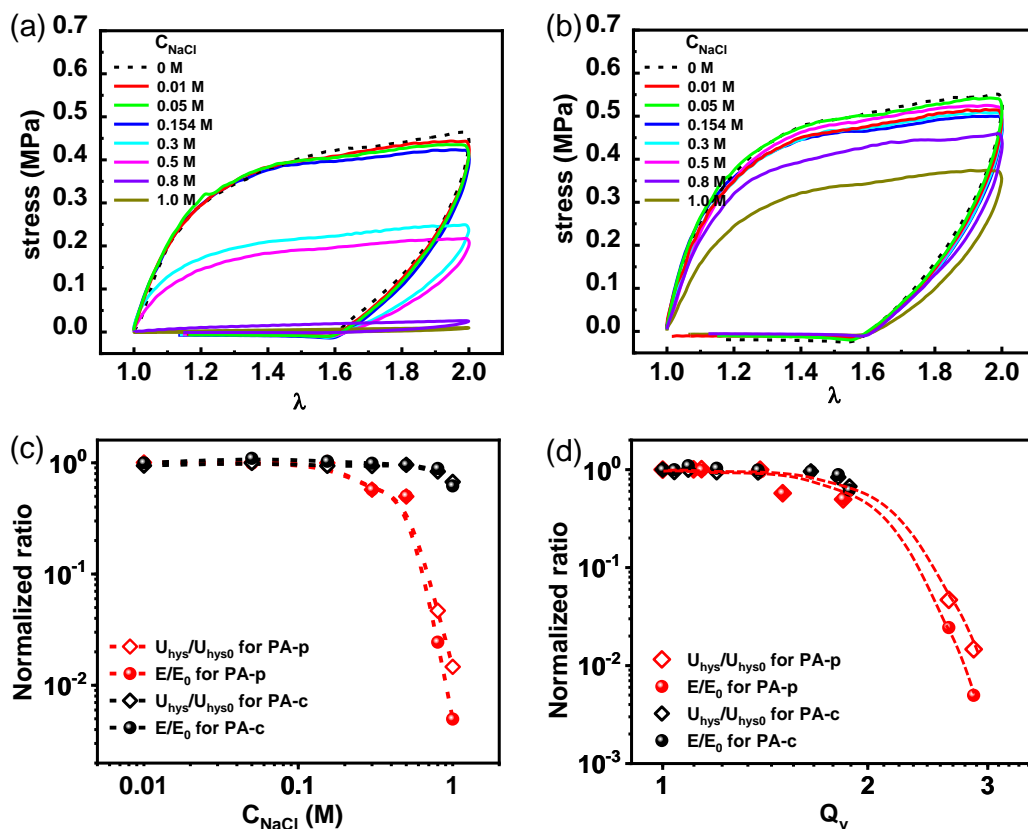

Figure 7. Reversibility of undeformed salt-equilibrated gels re-dialyzed in water to remove salt to reach water-reequilibrium. (**a-b**) Loading-unloading curves under nominal strain rate $\dot{\varepsilon} = 0.14$ s^{-1} for water-reequilibrated PA-p (a) and PA-c (b). The 0 M represents the pristine salt free gels. (**c-**

d) The normalized ratios of modulus E/E_0 and hysteresis energy density U_{hys}/U_{hys0} of the water-reequilibrated gels as a function of C_{NaCl} (c) and Q_v in saline solution (d). E_0 and U_0 are the modulus and hysteresis energy density for pristine salt-free gels. The dashed lines in (c) and (d) are a guide for the eyes.

CONCLUSIONS

Studying salt effect on tough hydrogels with ionic bonds is vitally important for their biological applications. We systematically investigated the dynamic mechanical behaviors in saline solution, using the dually crosslinked polyampholyte hydrogels as a model system. Two hydrogels dynamically crosslinked by ionic bonds were used: one is the physical hydrogel with the primary network crosslinked by topological entanglements, and in theory, the physical gel has no long-time modulus; and another one is the chemical hydrogel with the primary network crosslinked by chemical crosslinkers and trapped entanglements. Salt accelerated ionic bond dynamics, is equivalent to prolonging the observation time scale for salt-free gels. Thus, the salt effect can be considered as lowing frequency and reducing strain rate in rheology and large deformation tests, respectively, following the time-salt superposition principle. Accordingly, we can access a wide range of time scales (10^{-11} to 10^2 rad/s) at room temperature that is otherwise inaccessible for investigating the mechanical behaviors in water. The salt effect on mechanical properties (including shear and Young's moduli, fracture stretch ratio, hysteresis energy) can be efficiently converted into three rate-dependent regimes: (I) the high-frequency plateau regime from dynamic and primary networks, (II) viscoelastic regime from Sticky Rouse motion of ionic associations, and (III) the low-frequency plateau regime from the primary network. Specifically, comparing the experiment result with theoretical prediction value by the elastic network model, we revealed that disentanglement occurred in the physical gel in the regime III. Furthermore, the irreversibility of gels indicates the damage of primary and transient networks in saline solutions. The physical

mechanism revealed in this work gives important insight into toughening mechanism via dynamic bonds in other systems with dually crosslinked structures, and provides guidance for their practical applications in saline environment.

ASSOCIATED CONTENT

Supporting information

Figure S1. The appearance of equilibrated PA-p and PA-c (**a**) in water, and (**b**) in C_{NaCl} = 4 M solution.

Figure S2. Comparison between the norm of the complex shear modulus $|G^*|$ against $a_{salt}\omega$ from rheology test and the Young's modulus E against $2\pi a_{salt}\dot{\varepsilon}$ from uniaxial tensile test for (**a**) PA-p and (**b**) PA-c.

AUTHOR INFORMATION

Corresponding Author

*E-mail address: fengluo@scu.edu.cn (Feng Luo)

* E-mail address: gong@sci.hokudai.ac.jp (Jian Ping Gong)

Author Contributions

The manuscript was written by *X. L.*, *F. L.* and *J. P. G* with input of other authors. All authors have given approval to the final version of the manuscript. [#] *X.L. and F.L.* contributed equally to this work.

Notes

The authors declare no competing financial interest.

REFERENCES

(1) Gong, J. P.; Katsuyama, Y.; Kurokawa, T.; Osada, Y. Double‐network hydrogels with extremely high mechanical strength. *Adv. Mater.* **2003,** *15* (14), 1155-1158.

(2) Sun, J.-Y.; Zhao, X.; Illeperuma, W. R.; Chaudhuri, O.; Oh, K. H.; Mooney, D. J.; Vlassak, J. J.; Suo, Z. Highly stretchable and tough hydrogels. *Nature* **2012,** *489* (7414), 133–136.

(3) Hua, M.; Wu, S.; Ma, Y.; Zhao, Y.; Chen, Z.; Frenkel, I.; Strzalka, J.; Zhou, H.; Zhu, X.; He, X. Strong tough hydrogels via the synergy of freeze-casting and salting out. *Nature* **2021,** *590* (7847), 594-599.

(4) Guo, H.; Sanson, N.; Hourdet, D.; Marcellan, A. Thermoresponsive Toughening with Crack Bifurcation in Phase‐Separated Hydrogels under Isochoric Conditions. *Adv. Mater.* **2016,** *28* (28), 5857-5864.

(5) Liu, C.; Morimoto, N.; Jiang, L.; Kawahara, S.; Noritomi, T.; Yokoyama, H.; Mayumi, K.; Ito, K. Tough hydrogels with rapid self-reinforcement. *Science* **2021,** *372* (6546), 1078-1081.

(6) Nonoyama, T.; Lee, Y. W.; Ota, K.; Fujioka, K.; Hong, W.; Gong, J. P. Instant Thermal Switching from Soft Hydrogel to Rigid Plastics Inspired by Thermophile Proteins. *Adv. Mater.* **2020,** *32* (4), e1905878.

(7) Zhang, G.; Kim, J.; Hassan, S.; Suo, Z. Self-assembled nanocomposites of high water content and load-bearing capacity. *Proc Natl Acad Sci U S A* **2022,** *119* (32), e2203962119.

(8) Drury, J. L.; Mooney, D. J. Hydrogels for tissue engineering: scaffold design variables and applications. *Biomaterials* **2003,** *24* (24), 4337-4351.

(9) Zhao, X.; Chen, X.; Yuk, H.; Lin, S.; Liu, X.; Parada, G. Soft Materials by Design: Unconventional Polymer Networks Give Extreme Properties. *Chem. Rev.* **2021,** *121* (8), 4309-4372.

(10) Freedman, B. R.; Kuttler, A.; Beckmann, N.; Nam, S.; Kent, D.; Schuleit, M.; Ramazani, F.; Accart, N.; Rock, A.; Li, J. Enhanced tendon healing by a tough hydrogel with an adhesive side and high drug-loading capacity. *Nature Biomedical Engineering* **2022**, 1-13.

(11) Correa, S.; Grosskopf, A. K.; Lopez Hernandez, H.; Chan, D.; Yu, A. C.; Stapleton, L. M.; Appel, E. A. Translational applications of hydrogels. *Chem. Rev.* **2021,** *121* (18), 11385-11457.

(12) Blacklow, S.; Li, J.; Freedman, B.; Zeidi, M.; Chen, C.; Mooney, D. Bioinspired mechanically active adhesive dressings to accelerate wound closure. *Sci. Adv.* **2019,** *5* (7), eaaw3963.

(13) Yuk, H.; Varela, C. E.; Nabzdyk, C. S.; Mao, X.; Padera, R. F.; Roche, E. T.; Zhao, X. Dry double-sided tape for adhesion of wet tissues and devices. *Nature* **2019,** *575* (7781), 169-174.

(14) Yuk, H.; Lu, B.; Zhao, X. Hydrogel bioelectronics. *Chem. Soc. Rev.* **2019,** *48* (6), 1642-1667.

(15) Deng, J.; Yuk, H.; Wu, J.; Varela, C. E.; Chen, X.; Roche, E. T.; Guo, C. F.; Zhao, X. Electrical bioadhesive interface for bioelectronics. *Nat. Mater.* **2021,** *20* (2), 229-236.

(16) Tan, M.; Xu, Y.; Gao, Z.; Yuan, T.; Liu, Q.; Yang, R.; Zhang, B.; Peng, L. Recent Advances in Intelligent Wearable Medical Devices Integrating Biosensing and Drug Delivery. *Adv. Mater.* **2022**, 2108491.

(17) Creton, C. 50th Anniversary Perspective: Networks and Gels: Soft but Dynamic and Tough. *Macromolecules* **2017,** *50* (21), 8297-8316.

(18) Gong, J. P. Why are double network hydrogels so tough? *Soft Matter* **2010,** *6* (12), 2583.

(19) Wang, W.; Zhang, Y.; Liu, W. Bioinspired fabrication of high strength hydrogels from non-covalent interactions. *Prog. Polym. Sci.* **2017,** *71*, 1-25.

(20) Dai, X.; Zhang, Y.; Gao, L.; Bai, T.; Wang, W.; Cui, Y.; Liu, W. A Mechanically Strong, Highly Stable, Thermoplastic, and self‐healable supramolecular polymer hydrogel. *Adv. Mater.* **2015,** *27* (23), 3566-3571.

(21) Sun, T. L.; Kurokawa, T.; Kuroda, S.; Ihsan, A. B.; Akasaki, T.; Sato, K.; Haque, M. A.; Nakajima, T.; Gong, J. P. Physical hydrogels composed of polyampholytes demonstrate high toughness and viscoelasticity. *Nat. Mater.* **2013,** *12* (10), 932-937.

(22) Ihsan, A. B.; Sun, T. L.; Kurokawa, T.; Karobi, S. N.; Nakajima, T.; Nonoyama, T.; Roy, C. K.; Luo, F.; Gong, J. P. Self-healing behaviors of tough polyampholyte hydrogels. *Macromolecules* **2016,** *49* (11), 4245-4252.

(23) Long, T.; Li, Y.; Fang, X.; Sun, J. Salt-Mediated Polyampholyte Hydrogels with High Mechanical Strength, Excellent Self-Healing Property, and Satisfactory Electrical Conductivity. *Adv. Funct. Mater.* **2018,** *28* (44), 1804416.

(24) Luo, F.; Sun, T. L.; Nakajima, T.; Kurokawa, T.; Zhao, Y.; Sato, K.; Ihsan, A. B.; Li, X.; Guo, H.; Gong, J. P. Oppositely charged polyelectrolytes form tough, self-healing, and rebuildable hydrogels. *Adv. Mater.* **2015,** *27* (17), 2722-2727.

(25) Zhu, F.; Cheng, L.; Yin, J.; Wu, Z. L.; Qian, J.; Fu, J.; Zheng, Q. 3D Printing of Ultratough Polyion Complex Hydrogels. *ACS Appl Mater Interfaces* **2016,** *8* (45), 31304-31310.

(26) Hwang, J.; Cha, Y.; Ramos, L.; Zhu, T.; Buzoglu Kurnaz, L.; Tang, C. Tough antibacterial metallopolymer double-network hydrogels via dual polymerization. *Chem. Mater.* **2022,** *34* (12), 5663-5672.

(27) Guo, G.; Sun, J.; Wu, Y.; Wang, J.; Zou, L. Y.; Huang, J. J.; Ren, K.-F.; Liu, C.-M.; Wu, Z. L.; Zheng, Q. Tough complex hydrogels transformed from highly swollen polyelectrolyte hydrogels based on Cu 2+ coordination with anti-bacterial properties. *J. Mater. Chem. B* **2022,** *10* (34), 6414-6424.

(28) Fang, L.; Hu, J.; Zhang, C. W.; Wei, J.; Yu, H. C.; Zheng, S. Y.; Wu, Z. L.; Zheng, Q. Facile synthesis of tough metallosupramolecular hydrogels by using phosphates as temporary ligands of ferric ions to avoid inhibition of polymerization. *J. Polym. Sci.* **2022,** *60*, 2280-2288.

(29) Sun, T. L.; Luo, F.; Kurokawa, T.; Karobi, S. N.; Nakajima, T.; Gong, J. P. Molecular structure of self-healing polyampholyte hydrogels analyzed from tensile behaviors. *Soft matter* **2015,** *11* (48), 9355-9366.

(30) Sun, T. L.; Luo, F.; Hong, W.; Cui, K.; Huang, Y.; Zhang, H. J.; King, D. R.; Kurokawa, T.; Nakajima, T.; Gong, J. P. Bulk energy dissipation mechanism for the fracture of tough and self-healing Hydrogels. *Macromolecules* **2017,** *50* (7), 2923-2931.

(31) Luo, F.; Sun, T. L.; Nakajima, T.; King, D. R.; Kurokawa, T.; Zhao, Y.; Ihsan, A. B.; Li, X.; Guo, H.; Gong, J. P. Strong and Tough Polyion-Complex Hydrogels from Oppositely Charged Polyelectrolytes: A Comparative Study with Polyampholyte Hydrogels. *Macromolecules* **2016,** *49* (7), 2750-2760.

(32) Cui, K.; Sun, T. L.; Liang, X.; Nakajima, K.; Ye, Y. N.; Chen, L.; Kurokawa, T.; Gong, J. P. Multiscale energy dissipation mechanism in tough and self-healing hydrogels. *Phys. Rev. Lett.* **2018,** *121* (18), 185501.

(33) Cui, K.; Ye, Y. N.; Sun, T. L.; Chen, L.; Li, X.; Kurokawa, T.; Nakajima, T.; Nonoyama, T.; Gong, J. P. Effect of Structure Heterogeneity on Mechanical Performance of Physical Polyampholytes Hydrogels. *Macromolecules* **2019,** *52* (19), 7369-7378.

(34) Luo, F.; Sun, T. L.; Nakajima, T.; Kurokawa, T.; Zhao, Y.; Ihsan, A. B.; Guo, H. L.; Li, X. F.; Gong, J. P. Crack blunting and advancing behaviors of tough and self-healing polyampholyte hydrogel. *Macromolecules* **2014,** *47* (17), 6037-6046.

(35) Li, X.; Cui, K.; Sun, T. L.; Meng, L.; Yu, C.; Li, L.; Creton, C.; Kurokawa, T.; Gong, J. P. Mesoscale bicontinuous networks in self-healing hydrogels delay fatigue fracture. *Proc. Natl. Acad. Sci. U.S.A.* **2020,** *117* (14), 7606-7612.

(36) Li, X.; Cui, K.; Kurokawa, T.; Ye, Y. N.; Sun, T. L.; Yu, C.; Creton, C.; Gong, J. P. Effect of mesoscale phase contrast on fatigue-delaying behavior of self-healing hydrogels. *Sci. Adv.* **2021,** *7*, eabe8210.

(37) Li, X.; Gong, J. P. Role of dynamic bonds on fatigue threshold of tough hydrogels. *Proc. Natl. Acad. Sci. U.S.A.* **2022,** *119* (20), e2200678119.

(38) Haag, S. L.; Bernards, M. T. Polyampholyte Hydrogels in Biomedical Applications. *Gels* **2017,** *3* (4), 41.

(39) Roy, C. K.; Guo, H. L.; Sun, T. L.; Ihsan, A. B.; Kurokawa, T.; Takahata, M.; Nonoyama, T.; Nakajima, T.; Gong, J. P. Self-Adjustable Adhesion of Polyampholyte Hydrogels. *Adv. Mater.* **2015,** *27* (45), 7344-7348.

(40) Rao, P.; Sun, T. L.; Chen, L.; Takahashi, R.; Shinohara, G.; Guo, H.; King, D. R.; Kurokawa, T.; Gong, J. P. Tough hydrogels with fast, strong, and reversible underwater adhesion based on a multiscale design. *Adv. Mater.* **2018,** *30* (32), 1801884.

(41) Cui, K.; Ye, Y. N.; Sun, T. L.; Yu, C.; Li, X.; Kurokawa, T.; Gong, J. P. Phase separation behavior in tough and self-healing polyampholyte hydrogels. *Macromolecules* **2020,** *53* (13), 5116-5126.

(42) Spruijt, E.; Sprakel, J.; Lemmers, M.; Stuart, M. A.; van der Gucht, J. Relaxation dynamics at different time scales in electrostatic complexes: time-salt superposition. *Phys. Rev. Lett.* **2010,** *105* (20), 208301.

(43) Nisato, G.; Munch, J. P.; Candau, S. J. Swelling, Structure, and Elasticity of Polyampholyte Hydrogels. *Langmuir* **1999,** *15* (12), 4236-4244.

(44) English, A. E.; Mafé, S.; Manzanares, J. A.; Yu, X.; Grosberg, A. Y.; Tanaka, T. Equilibrium swelling properties of polyampholytic hydrogels. *The Journal of Chemical Physics* **1996,** *104* (21), 8713-8720.

(45) Dobrynin, A. V.; Colby, R. H.; Rubinstein, M. Scaling theory of polyelectrolyte solutions. *Macromolecules* **1995,** *28* (6), 1859-1871.

(46) Zhang, Z.; Chen, Q.; Colby, R. H. Dynamics of associative polymers. *Soft Matter* **2018,** *14* (16), 2961-2977.

(47) Cui, K.; Gong, J. P. How double dynamics affects the large deformation and fracture behaviors of soft materials. *J. Rheol.* **2022,** *66* (6), 1093-1111.

(48) Rubinstein, M.; Colby, R. H., *Polymer Physics*. Oxford University Press: New York, 2003; Vol. 23.

(49) Ferry, J. D., *Viscoelastic properties of polymers*. 3rd ed. ed.; John Wiley & Sons: New York, 1980.

(50) Higgs, P. G.; Joanny, J. F. Theory of polyampholyte solutions. *J. Chem. Phys.* **1991,** *94* (2), 1543-1554.